Heliyon 10 (2024) e24695

Contents lists available at ScienceDirect

Heliyon

journal homepage: www.cell.com/heliyon

Research article

Danggui Jixueteng decoction for the treatment of myelosuppression after chemotherapy: A combined metabolomics and network pharmacology analysis

Mingxin Guo [a,1], Jiaqi Zeng [a,1], Wenjing Li [b], Zhiqiang Hu [a], Ying Shen [a,*]

[a] Department of Pharmacy, The Affiliated Yixing Hospital of Jiangsu University, Yixing, 214200, China
[b] School of Pharmacy, Qiqihar Medical University, Qiqihaer, 161006, China

ARTICLE INFO

Keywords:
Danggui Jixueteng decoction
Myelosuppression after chemotherapy
Network pharmacology
Molecular docking
Hematopoietic microenvironment

ABSTRACT

Objective: This study aimed to explore the mechanism of the Danggui Jixueteng decoction (DJD) in treating Myelosuppression after chemotherapy (MAC) through network pharmacology and metabolomics.

Methods: We obtained the chemical structures of DJD compounds from TCMSP and PubMed. SwissTargetPrediction, STITCH, CTD, GeneCards, and OMIM were utilized to acquire component targets and MAC-related targets. We identified the key compounds, core targets, main biological processes, and signaling pathways related to DJD by constructing and analyzing related networks. The main active compounds and key proteins of DJD in treating AA were confirmed by molecular docking. A MAC rat model was established through intraperitoneal injection of cyclophosphamide to confirm DJD's effect on the bone marrow hematopoietic system. Untargeted metabolomics analyzed serum metabolite differences between MAC rats and the control group, and before and after DJD treatment, to explore DJD's mechanism in treating MAC.

Results: Of the 93 active compounds identified under screening conditions, 275 compound targets and 3113 MAC-related targets were obtained, including 95 intersecting targets; AKT1, STAT3, CASP3, and JUN were key proteins in MAC treatment. The phosphatidylinositol-3-kinase/RAC-alpha serine/threonine-protein kinase (PI3K/AKT) signaling pathway may play a crucial role in MAC treatment with DJD. Molecular docking results showed good docking effects of key protein AKT1 with luteolin, β-sitosterol, kaempferol, and glycyrrhizal chalcone A. *In vivo* experiments indicated that, compared to the model group, in the DJD group, levels of WBCs, RBCs, HGB, and PLTs in peripheral blood cells, thymus index increased, spleen index decreased, serum IL-3, GM-CSF levels increased, and IL-6, TNF-α, and VEGF levels decreased ($p < 0.01$); the pathological morphology of femoral bone marrow improved. Eleven differential metabolites were identified as differential serum metabolites, mainly concentrated in phenylalanine, tyrosine, and tryptophan biosynthesis pathways, phenylalanine metabolism, and arachidonic acid metabolism.

Conclusion: This study revealed that DJD's therapeutic effects are due to multiple ingredients, targets, and pathways. DJD may activate the PI3K/AKT signaling pathway, promote hematopoietic-related cytokine production, regulate related metabolic pathways, and effectively alleviate cyclophosphamide-induced myelosuppression after chemotherapy in rats.

* Corresponding author.
E-mail address: staff773@yxph.com (Y. Shen).
[1] These authors contributed equally to this works.

https://doi.org/10.1016/j.heliyon.2024.e24695
Received 1 September 2023; Received in revised form 11 January 2024; Accepted 12 January 2024
Available online 19 January 2024

1. Introduction

The prevalence of cancer increases annually, accompanied by frequent treatment side effects. A common clinical side effect is myelosuppression after chemotherapy (MAC) [1]. Post-chemotherapy, bone marrow suppression not only diminishes patients' quality of life but can also pose a health threat. Ongoing experimental investigations aim to understand MAC's pathophysiology and identify pharmacological treatments. Although biological agents and blood products can significantly improve MAC, they have limitations, such as single-target actions and numerous adverse reactions [2]. Traditional Chinese medicine (TCM) compounds often engage multiple targets, potentially increasing efficacy, reducing toxicity, alleviating clinical symptoms, and improving quality of life [3]. However, the chemical basis and mechanisms of TCM substances in treating MAC are under-explored. Thus, identifying the relationship between TCM prescriptions and disorders remains a key objective in clinical drug therapy and research.

Danggui Jixueteng Decoction (DJD), derived from the book "Traditional Chinese Medicine Traumatology," consists of six TCM: Angelica sinensis radix, Spatholobi Caulis, Rehmanniae radix praeparata, Longan arillus, Paeoniae radix alba, and Salviae Miltiorrhizae Radix et Rhizoma. Known for its efficacy in replenishing qi, activating blood, invigorating blood circulation, removing blood stasis, and relieving pain, DJD is extensively used for treating frozen shoulder, cervical spondylosis, and heel pain [4,5]. Modern Chinese medicine categorizes MAC as "blood deficiency." Each DJD component has varying degrees of beneficial and activating effects on blood. Angelicae sinensis radix and Salviae Miltiorrhizae Radix et Rhizoma are particularly noted for alleviating anemia's clinical symptoms and indicators [6,7]. However, reports on DJD treating MAC are scarce, and its potential mechanism and active compounds remain unclear. This study explored DJD's drug targets, disease treatment mechanisms, and signaling pathways, employing traditional molecular experiments and innovative network pharmacology. Chemometrics simulated the geometric and energy matching of molecules to identify optimal binding modes between small molecule ligands and biological macromolecule receptors [8]. The advancement of computer-aided technologies like network pharmacology and molecular docking has compensated for the long cycle, high effort, and low efficiency of traditional TCM research techniques, significantly enhancing the development of new pharmaceuticals [9]. Systems biology, crucial in metabolomics technology, analyzes metabolite changes in human fluids, tissues, and organs, providing insights into pathogenic mechanisms and therapeutic actions [10,11].

This study, based on network pharmacology, molecular docking, and metabolomics, investigated the main active components, key targets, pathways, and mechanisms of DJD in MAC treatment. It supports further exploration of DJD as a potential MAC treatment and provides a theoretical foundation for its application in treating myelosuppression after chemotherapy.

2. Materials and methods

2.1. Chemical reagents and herbal materials

Q Exactive HF LC/MS (Thermo); LC-MS grade acetonitrile, methanol and formic acid (Merck KGaA, UK). XN9500 automatic blood analyzer (Japan, Sysmex); SIMCA-P 14.0 (Sweden, Umetrics); Cyclophosphamide (Shanghai Yuanye Biotechnology Co., LTD); Interleukin-3 (IL-3)(20231015R012), Interleukin-6(IL-6)(20230505R251), Granulocyte macrophage colony stimulating factor (GM-CSF)(20230316R097), tumor necrosis factor-α (TNF-α)(20230316R097), and vascular endothelial growth factor (VEGF) (20230505R168) lisa kits (Jiangsu Meimian Industrial Co., LTD). Angelica sinensis radix (230504841), Spatholobi Caulis (230304161), Rehmanniae radix praeparata (230200039), longan arillus (230304341), Paeoniae radix alba (230400229), and Salviae Miltiorrhizae Radix et Rhizoma (230600031) (Kangmei Pharmaceutical Co., LTD) were identified by pharmacists according to the standards of Chinese Pharmacopoeia. Other reagent is analytical pure, water is ultrapure water.

2.2. Network pharmacology prediction

Active compounds and targets of Angelicae sinensis radix, Spatholobi Caulis, Rehmanniae Radix Praeparata, Paeoniae Radix Alba, and Salviae Miltiorrhizae Radix et Rhizoma were identified using TCMSP (https://tcmspw.com/tcmsp.php) [12]. For longan arillus, active compounds were searched in databases including CNKI, VIP, Wanfang, PubMed, and Web of Science. The SMILES structure of longan arillus was uploaded to the Swiss Target Prediction database (https://www.swisstargetprediction.ch/) for target forecasting [13]. The format of medication active compounds and target information was standardized using the DrugBank database (https://www.drugbank.ca/) [14].

Keywords "myelosuppression after chemotherapy" and "bone marrow suppression" were used to search the GeneCards Human Gene Database (https://genealacart.genecards.org/) [15], the Online Mendelian Inheritance in Man (OMIM) database (https://www.omim.org/) [16], the Pharmacogenomics Knowledge Base (PharmGKB) (https://www.pharmgkb.org/) [17], and the Therapeutic Target Database (http://db.idrblab.net/ttd/) [18]. After combining target genes from each database, duplicates and false positives were removed. The remaining disease target genes were refined using the UniProt database to yield candidate target genes.

Protein interactions of DJD in treating MAC were examined using the STRING database (https://string-db.org/) [19]. The PPI network diagram was created with Homo sapiens as the species. This study used network topology from PPI entries generated by the STRING database and analyzed with Cytoscape3.9.1 software. Key nodes in the network were identified with degree centrality and betweenness centrality greater than the median of the group and closeness centrality greater than the average of the group as indicators. These are the main proteins involved in DJD's treatment of MAC.

Ninety-five overlapping target genes were used for enrichment and analysis of cell composition, molecular function, biological

process, and signaling pathways using the DAVID Functional Annotation Tools (https://David.Ncifcrf.gov/). Visualization was facilitated by the micro-information platform (https://www.bioinformatics.com.cn/).

2.3. Molecular docking of the active compounds with the target protein

Three-dimensional structures of luteolin, β-sitosterol, kaempferol, and glycyrrhizic chalcone A were sourced from the PubChem database (https://pubchem.ncbi.nlm.nih.gov/). Protein target three-dimensional structures were obtained from the RCSB PDB database (https://www.rcsb.org/) [20]. Preliminary analyses of protein receptors and active compounds were conducted using AutoDock Vina molecular docking software. Subsequently, molecular docking simulations were performed to calculate docking binding energies and generate a docking heatmap.

2.4. Preparation of DJD

As per "Traditional Chinese Medicine Traumatology," 15 g each of Angelicae sinensis radix, Spatholobi Caulis, and Rehmanniae Radix Praeparata, 9 g each of Salviae Miltiorrhizae Radix et Rhizoma and Paeoniae Radix Alba, and 6 g of longan arillus were weighed. The medicinal materials were soaked in 2 L of pure water for 1 h, then brought to a boil and decocted for 30 min. The decoction was filtered, and the residue was reboiled with six times the amount of distilled water for 30 min and filtered again. Both filtrates were combined and concentrated under reduced pressure in a rotary evaporator to produce the test solution.

2.5. Animal model

The animal study adhered to the guidelines for the care and use of laboratory animals published by the US National Academy of Sciences and the US National Institutes of Health, along with the principles of laboratory animal care established by the National Institute for Medical Research. The study was conducted in line with the ARRIVE guidelines. All animal experiments were approved by the Institutional Animal Care and Use Committee (approval number: QMU-AECC-2023-88).

Male SD rats, 7 weeks old and weighing approximately 180–220 g, were sourced from Beijing Vitonglihua Experimental Animal Technology Co., Ltd. (Beijing, China). The rats were housed under typical laboratory conditions with 12 h of darkness and 12 h of light, and had free access to food and water. After a week of acclimatization, thirty-six rats were randomly divided into six groups ($n = 6$): blank group (healthy), model group (myelosuppression after chemotherapy), positive drug group (Ejiao syrup, 10.8 g kg^{-1}), DJD-L group (3.10 g kg^{-1}), DJD-M group (6.21 g kg^{-1}), and DJD-H group (12.42 g kg^{-1}). The MAC model was induced by intraperitoneal injection of 30 mg/kg cyclophosphamide solution for 5 days, excluding the normal group. Concurrently, each group received oral gavage at the designated dose once daily for 15 days, while the blank and model groups were administered the same volume of normal saline. 24 h after the final DJD treatment, all rats were euthanized. Samples were collected and stored as per relevant testing requirements.

2.6. Sample collection

An intraperitoneal dose of 3 % pentobarbital sodium (30 mg kg^{-1}) was used for rat anesthesia [21]. Post successful anesthesia, 3–5 mL of blood was drawn from the venous plexus of the inner canthus and collected in a test tube. Blood samples in anticoagulant tubes were immediately analyzed using an automated biochemical analyzer. The blood samples in test tubes were stored at 4 °C for 2 h, then centrifuged at 4500 r·min^{-1} for 10 min, and the supernatant was collected. Following blood collection, rats were euthanized by cervical dislocation, and the femurs were removed aseptically, along with the muscles.

2.7. Peripheral blood cell counts in rats

Blood samples were collected from the intraocular venous plexus of anesthetized rats. The anticoagulant used in the blood samples was EDTA-2K. An automated biochemical analyzer was employed to determine the levels of RBCs, WBCs, HGB, and PLTs in the blood [22].

2.8. Organ index measurement

The thymus and spleen were removed from the euthanized rats, rinsed with cold normal saline, dried with filter paper, and weighed. The organ index is calculated as the ratio of organ mass to the total body mass of the animal [23].

2.9. Bone marrow tissue pathology observation

Rats were euthanized via cervical dislocation. The right fibula was promptly excised under aseptic conditions and immersed in fixation solution (comprising 100 mL of paraformaldehyde and 5.5 g of EDTA). After 15–20 days at 4 °C, bone marrow tissue was embedded in paraffin, stained with HE, and observed under an optical microscope.

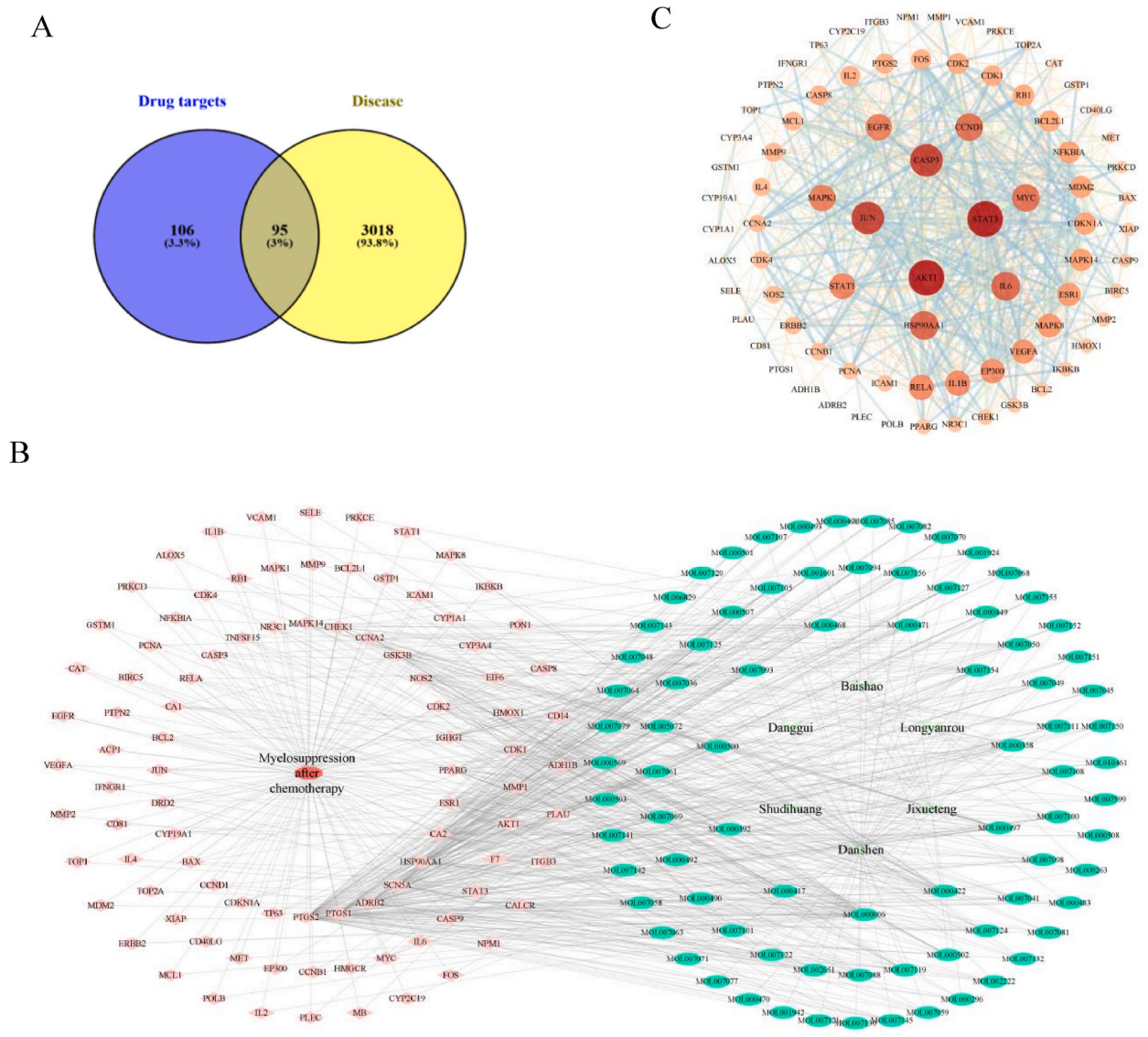

Fig. 1. Regulatory networks of DJD compounds correspond to potential MAC targets. (A) The intersection of DJD compound targets and MAC targets. (B) Network diagram of "compounds-targets-disease". Red ellipses represent diseases, pink diamonds represent target genes that intersect those diseases, green triangles represent traditional Chinese medicine compounds in DJD, and green ellipses represent active compounds. (C) The protein interaction network of DJD in the treatment of MAC targets. with rounded nodes designating proteins and lines designating protein interactions.

2.10. Enzyme-linked immunosorbent assay

Blood samples were collected from the inner canthus venous plexus of anesthetized rats, and serum samples were obtained after storage at 4 °C for 3 h. The serum levels of IL-3, IL-6, GM-CSF, VEGF, and TNF-α were measured using ELISA kits.

2.11. Metabonomics research

Serum samples from the blank group, the model group, and the DJD-H group were used as metabonomics test samples. Equal quantities of samples were mixed to create the quality control (QC) sample.

2.11.1. Liquid phase and mass spectrometry conditions

Chromatographic Conditions: Chromatographic separation was conducted on a Q Exactive HF LC/MS using a Zorbax Eclipse C18 column (1.8 μm × 2.1 mm × 100 mm). The column temperature was maintained at 30 °C, and the flow rate was set at 0.3 mL/min. The

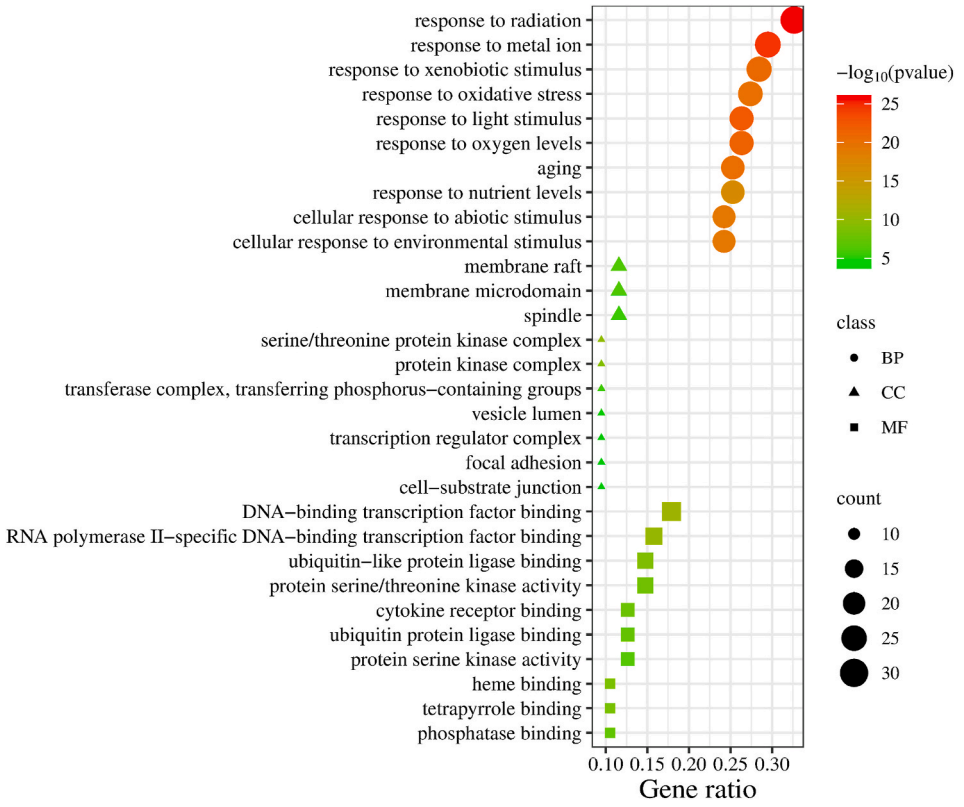

Fig. 2. GO enrichment analyses. The item name appears in the ordinate, the number of target genes ratio on the item appears in the abscissa, and the color represents the *P* value.

mobile phase composition comprised A: 0.1 % formic acid solution and B: pure acetonitrile. The injection volume was 2 μL, and the autosampler temperature was kept at 4 °C. The serum sample gradient was as follows: 0–2.0 min at 5 % B; 2.0–6.0 min at 5–30 % B; 6.0–7.0 min at 30 % A; 7.0–12.0 min at 30–78 % B; 12.0–14.0 min at 78 % B; 14.0–17.0 min at 78–95 % B; 17.0–20.0 min at 95 % B.

Mass Spectrometry Conditions: The optimized MS conditions were: Positive and negative modes; heater temperature at 325 °C; sheath gas flow at 45 arb; auxiliary gas flow at 15 arb; sweep gas flow at 1 arb; electrospray voltage at 3.5 KV; capillary temperature at 330 °C; S-Lens RF Level at 55 %. The scanning mode included a full scan (*m/z* 100–1500) and data-dependent mass spectrometry (dd-MS2, TopN = 5); resolution was 120,000 (MS1) & 60,000 (MS2). The collision mode used was High-Energy Collision Dissociation (HCD).

2.11.2. Metabolomics data processing

The raw data from mass spectrometry analysis were processed for retention time correction, peak identification, extraction, integration, and alignment, creating a data matrix linked to metabolites. Metabolomics data for two ion modes were obtained. The data were then analyzed using SIMCA 14.1 software for multidimensional statistical analysis, including principal component analysis (PCA) and orthogonal partial least squares discriminant analysis (OPLS-DA). Differential metabolites between the blank group and the model group, as well as between the DJD group and the model group, were screened based on VIP (variable impact in the project) > 1.0 and $P < 0.05$. Drug recall observations and database consultations were performed for final inclusion. Metabolite data were imported into MetaboAnalyst 5.0 (http://www.metaboAnalyst.ca/) for metabolic pathway enrichment analysis to identify pathways related to MAC.

2.12. Statistical processing method

Data are presented as mean ± SD. Statistical analyses were performed using SPSS PRO (https://spsspro.com). One-way ANOVA was applied for group comparisons. p-values less than 0.05 were considered statistically significant.

3. Results

3.1. Regulatory network of potential targets corresponding to DJD compounds

Utilizing "Angelicae sinensis radix, Spatholobi Caulis, Rehmanniae Radix Praeparata, longan arillus, Paeoniae Radix Alba, and

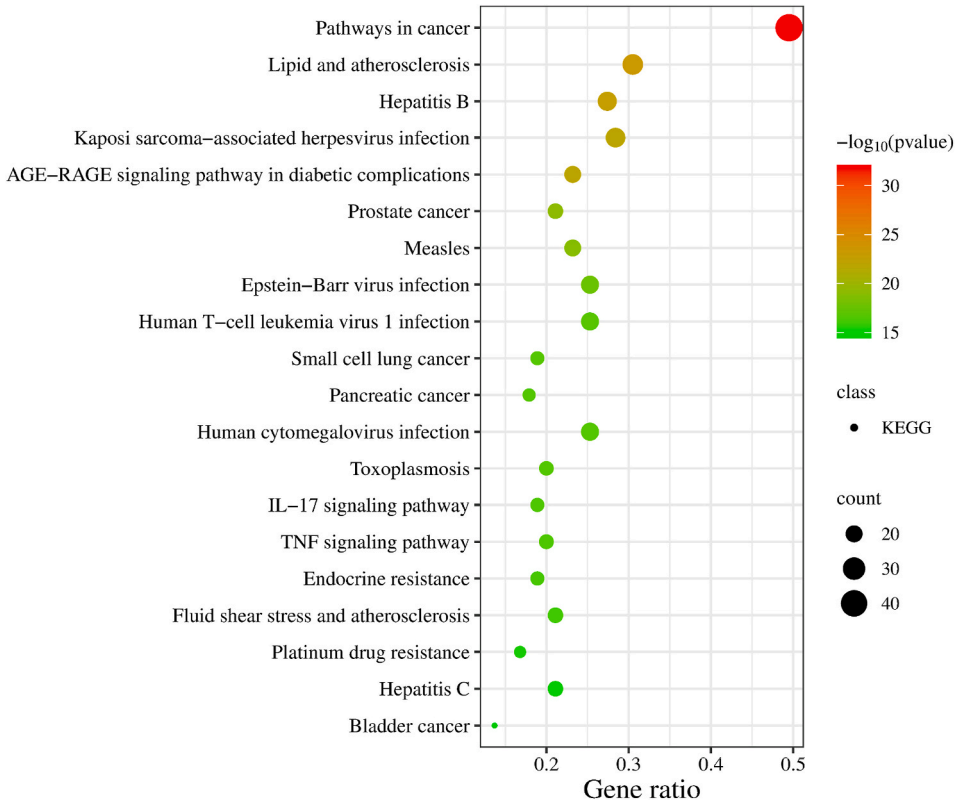

Fig. 3. KEGG enrichment analyses. The item name appears in the ordinate, the number of target genes enriched on the item appears in the abscissa, and the color represents the P value.

Salviae Miltiorrhizae Radix et Rhizoma" as keywords, 93 active compounds and 201 corresponding targets were identified from the TCMSP database. Employing "MAC" as the keyword, 3113 MAC-related targets were searched for in the GeneCards, OMIM, PharmGKB, and TTD databases. Fig. 1A illustrates that 95 common targets were identified following the intersection of compound targets and MAC targets.

3.2. Constructing a "compounds-targets-disease" network

A "compounds-targets-disease" network diagram of DJD and MAC was created using Cytoscape 3.9.1, shown in Fig. 1B. The network comprised 183 nodes and 718 edges, with each edge representing the interaction between active compounds and intersecting targets. Multiple traditional Chinese medicine components impacted multiple targets, and numerous compounds simultaneously affected the same target. Through network topology analysis, active compounds were ranked by degree. Luteolin was connected to 44 targets, β-sitosterol to 44 targets, kaempferol to 39 targets, and glycyrrhiza chalcone A to 39 targets, with additional details provided in Table S1. These findings suggest these active compounds play a crucial role in MAC treatment.

3.3. PPI network development and core protein screening

We entered the 95 intersecting targets into the STRING database and developed a PPI network, depicted in Fig. 1C, to predict target interconnections and identify crucial proteins. Key nodes in the network were screened based on the criteria that degree centrality was greater than the median, and medium centrality and tight centrality were above the average. AKT1, STAT3, CASP3, and JUN interact with 44, 44, 39, and 39 proteins, respectively, and are considered key proteins of DJD in MAC treatment.

3.4. GO and KEGG enrichment analyses

A total of 3391 GO items were enriched, including 1808 biological process entries, 123 molecular function entries, and 1460 cell component entries. The top ten enriched items were selected, and histograms were generated for each item based on their P value, Q value, and gene count, as shown in Fig. 2. Additionally, 149 KEGG signaling pathways were identified. The top 20 enriched items were chosen, and histograms were plotted according to P value, Q value, and gene count. The key pathways implicated in DJD's treatment of MAC, as depicted in Fig. 3, included human T-cell leukemia virus, lipid and atherosclerosis signaling pathway, TNF signaling pathway,

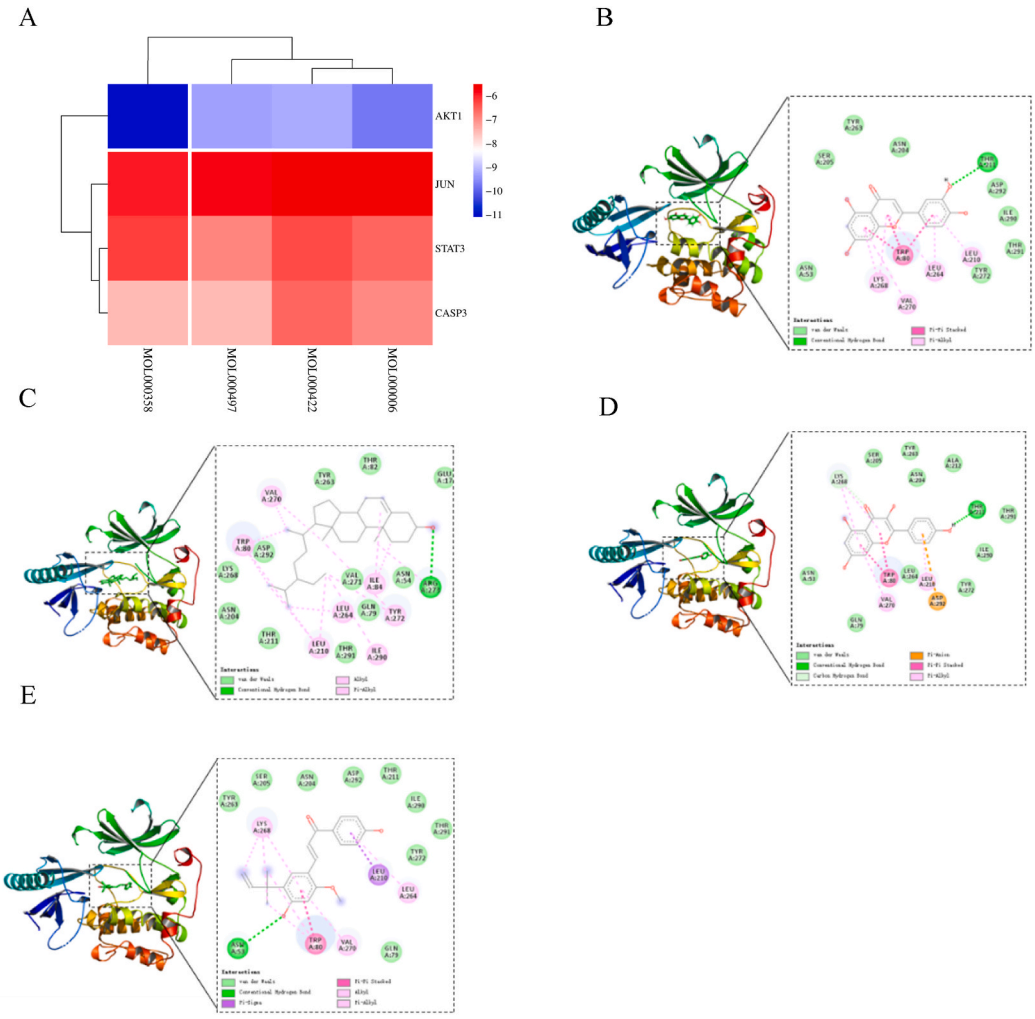

Fig. 4. Molecular docking diagram between the target and the active compounds. (A) Molecular docking thermogram. (B) AKT protein docked with luteolin. (C) AKT protein docked with β-sitosterol. (D) AKT protein docked with kaempferol. (E) AKT protein docked with glycyrrhiza chalcone A.

human cytomegalovirus, and IL-17 signaling pathway.

3.5. *"Active compounds-target" molecular docking*

Molecular docking verification of luteolin, β-sitosterol, kaempferol, and glycyrrhiza chalcone A with proteins AKT1, STAT3, CASP3, and JUN was conducted using AutoDock Vina. The binding energy was the assessment metric, where lower binding energy indicated a more effective docking effect. Each active component showed a binding energy of less than −4 kcal/mol with distinct core proteins, as shown in Fig. 4A. Docking with AKT1 had the lowest binding energy, underscoring DJD's influence on AKT1 in MAC treatment, as illustrated in Fig. 4B–E.

3.6. *Experimental verification of DJD treatment in MAC model rats*

3.6.1. *Effect on body mass*

Comparing the conditions of rats in each group revealed that rats in the model group exhibited poor health and significantly reduced activity. Their coats were gray and fluffy, with gray lips and auricles, pale limbs, and significantly decreased body mass. In contrast, each treatment group, including those treated with DJD, showed notable improvements in mental state, coat color, and body mass. After 7 days of intervention, body mass began to increase gradually, with a significant increase observed on the 15th day, as indicated in Fig. 5A ($P < 0.01$). These results demonstrate that DJD can improve the condition and body mass of MAC model rats.

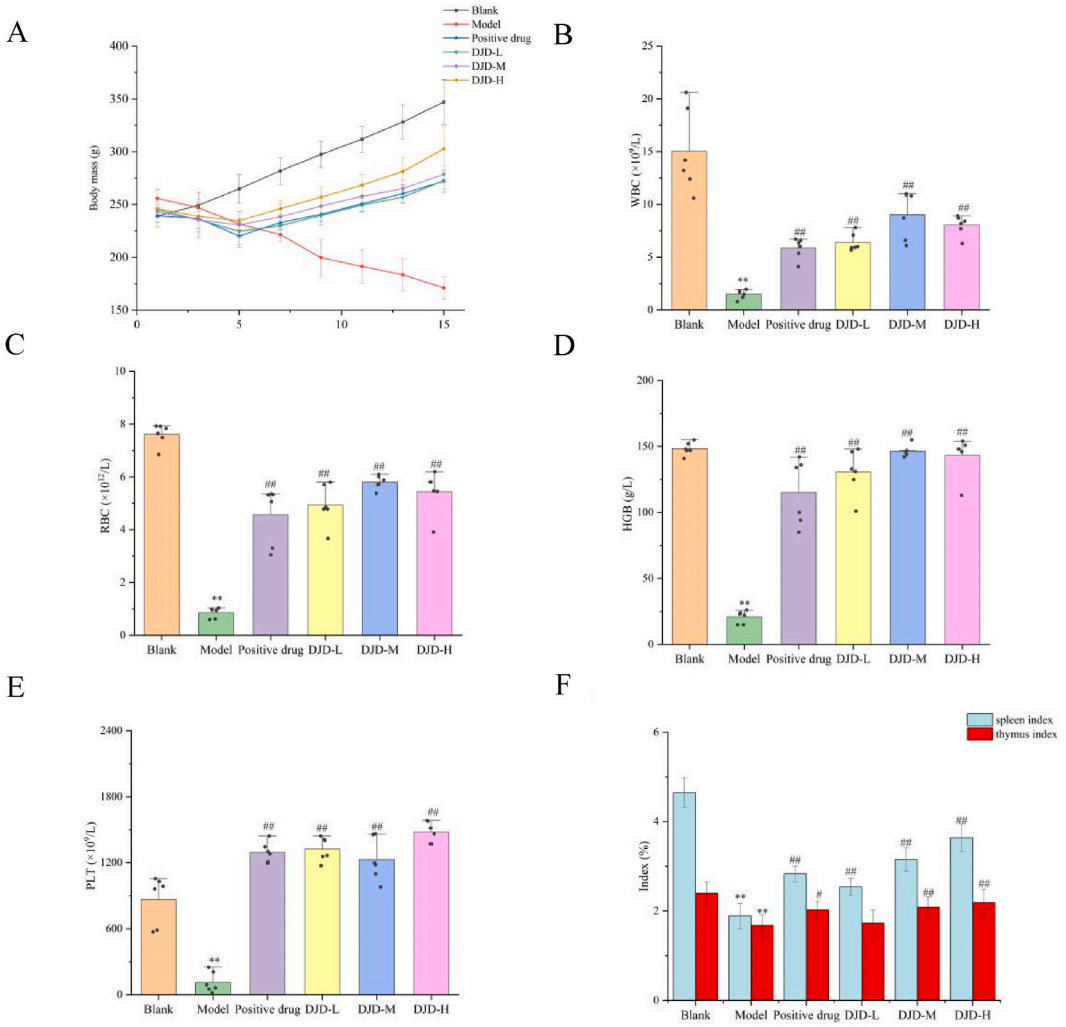

Fig. 5. Effect of DJD on the body weight of MAC model rats, peripheral blood flow, and organ index. (A) Effect of DJD on the body mass of MAC model rats. (B) Effect of DJD on the number of WBCs in MAC model rats. (C) Effect of DJD on the number of RBCs in MAC model rats. (D) Effect of DJD on HGB levels in MAC model rats. (E) Effect of DJD on PLTs numbers in MAC rats. (F) Effect of DJD on the spleen index and thymus index of MAC rats. Compared with the control group, $^{**}P < 0.01$, compared with the model group, $\#P < 0.05$, $\#\#P < 0.01$, the same below.

3.6.2. Effect on the peripheral blood cell counts and organ index

In comparison to the control group, the peripheral blood levels of WBCs, RBCs, HGB, and PLTs in the model group rats were significantly reduced ($P < 0.05$, $P < 0.01$). These levels in MAC model rats treated with Ejiao syrup and DJD exhibited a significant increase, as shown in Fig. 5B–E. These indices differed significantly from those in the model group ($P < 0.05$). DJD effectively improved peripheral hemogram indices in MAC model rats. Post-dissection and weighing of the thymus and spleen, it was observed that the thymus index and spleen index in MAC model rats decreased significantly ($P < 0.01$). Compared to the model group, the thymus index and spleen index in the Positive drug (Ejiao syrup, 10.8 g kg^{-1}), DJD-M (6.21 g kg^{-1}), and DJD-H (12.42 g kg^{-1}) groups increased significantly ($P < 0.05$, $P < 0.01$). The thymus index in the DJD-L (3.10 g kg^{-1}) group showed no significant change (Fig. 5F, $P > 0.05$).

3.6.3. Effect on pathomorphology of bone marrow

Fig. 6 depicts the bone marrow structure in various groups. In the blank group, the medullary cavity structure was clear, with visible hematopoietic tissue and capillaries, abundant nucleated cells, and red blood cells, but no adipocytes. In the model group, the number of hematopoietic-associated cells in the bone marrow cavity was markedly reduced compared to the control group, with the medullary cavity filled with adipose tissue and evident fibrosis. Each administration group, particularly the DJD-M and DJD-H groups, showed an increased number of nucleated cells in the bone marrow compared to the model group. The number of adipocytes decreased, and the pathological damage to the bone marrow was significantly mitigated. DJD improved pathological injury in MAC model rats.

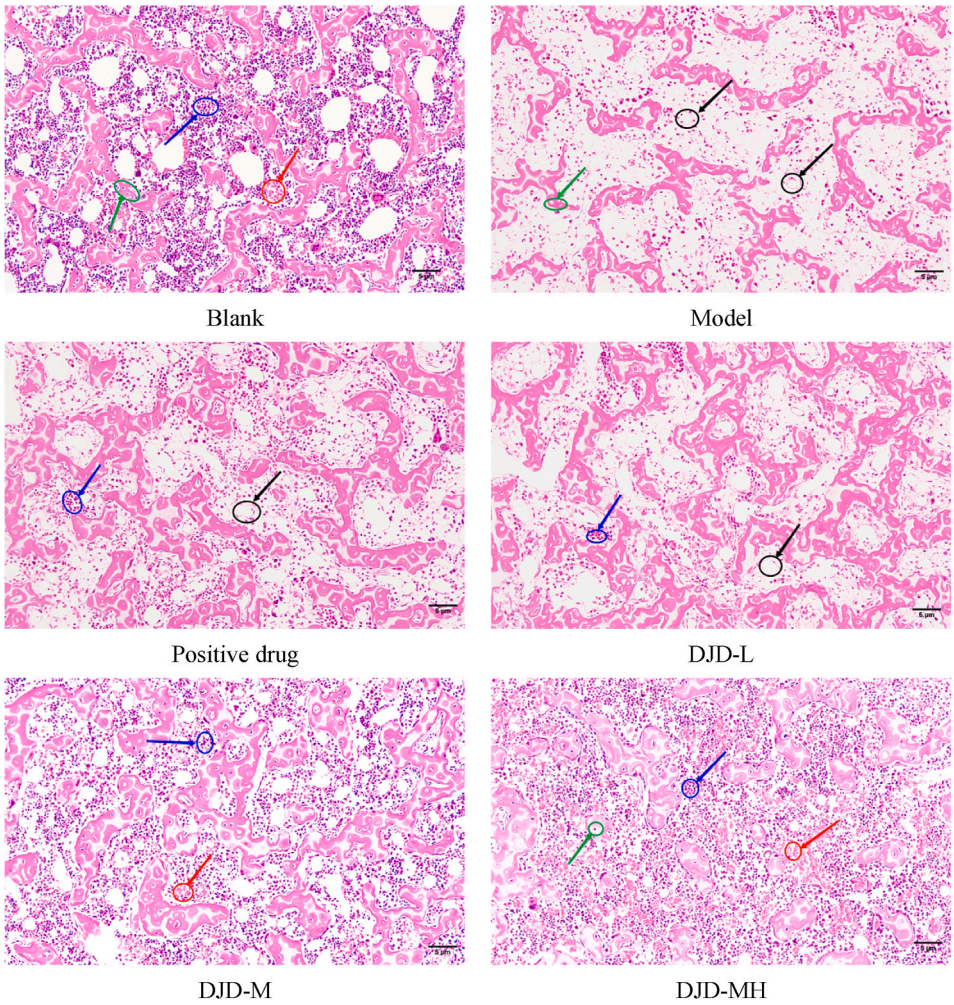

Fig. 6. Morphological and structural changes in the bone marrow of each group of rats. Blue arrow: nucleated cells, red arrow: red blood cells, black arrow: adipocytes, green arrow: hematopoietic tissue and capillaries. (× 200)

3.6.4. Effect of DJD on the expression of IL-3, IL-6, GM-SCF, TNF-α, and VEGF

ELISA was employed to measure the levels of IL-3, IL-6, GM-CSF, TNF-α, and VEGF in the peripheral blood of each rat. Compared to the control group, the model group exhibited significantly increased levels of TNF-α, IL-6, and VEGF, while the levels of IL-3 and GM-CSF were significantly reduced. As depicted in Fig. 7A–E, after 15 days of DJD treatment, the expression levels of TNF-α, IL-6, and VEGF significantly decreased compared to the model group, while the levels of IL-3 and GM-CSF significantly increased ($P < 0.05$, $P < 0.01$). Additionally, the levels of GM-CSF and VEGF showed no significant difference between the model group and the DJD-L group.

3.7. Analysis of serum metabonomics in MAC model rats intervened by DJD

3.7.1. Multivariate statistical analysis

PCA and OPLS-DA were used to evaluate serum data from the blank, model, and DJD groups. The PCA results, shown in Fig. 8A–F, indicate a high degree of aggregation of QC samples in both positive and negative ion modes, confirming the stability and repeatability of the experimental method. There was a discernible differentiation tendency among the experimental groups. The separation of samples from the blank control group and the model group indicated successful grouping into two distinct categories, suggesting the effective establishment of the bone marrow suppression model post-cyclophosphamide injection. The OPLS-DA analysis demonstrated clear distinctions in the serum metabolic profiles of the three groups. The data model underwent 200 permutation tests, yielding R2 = 0.705 and Q2 = −0.472 in positive ion mode and R2 = 0.843 and Q2 = −0.529 in negative ion mode, indicating no overfitting in the model.

3.7.2. Screening of differential metabolites

Differential metabolites were identified using the criteria of VIP >1.0 and $P < 0.05$. In the comparison between the blank group and

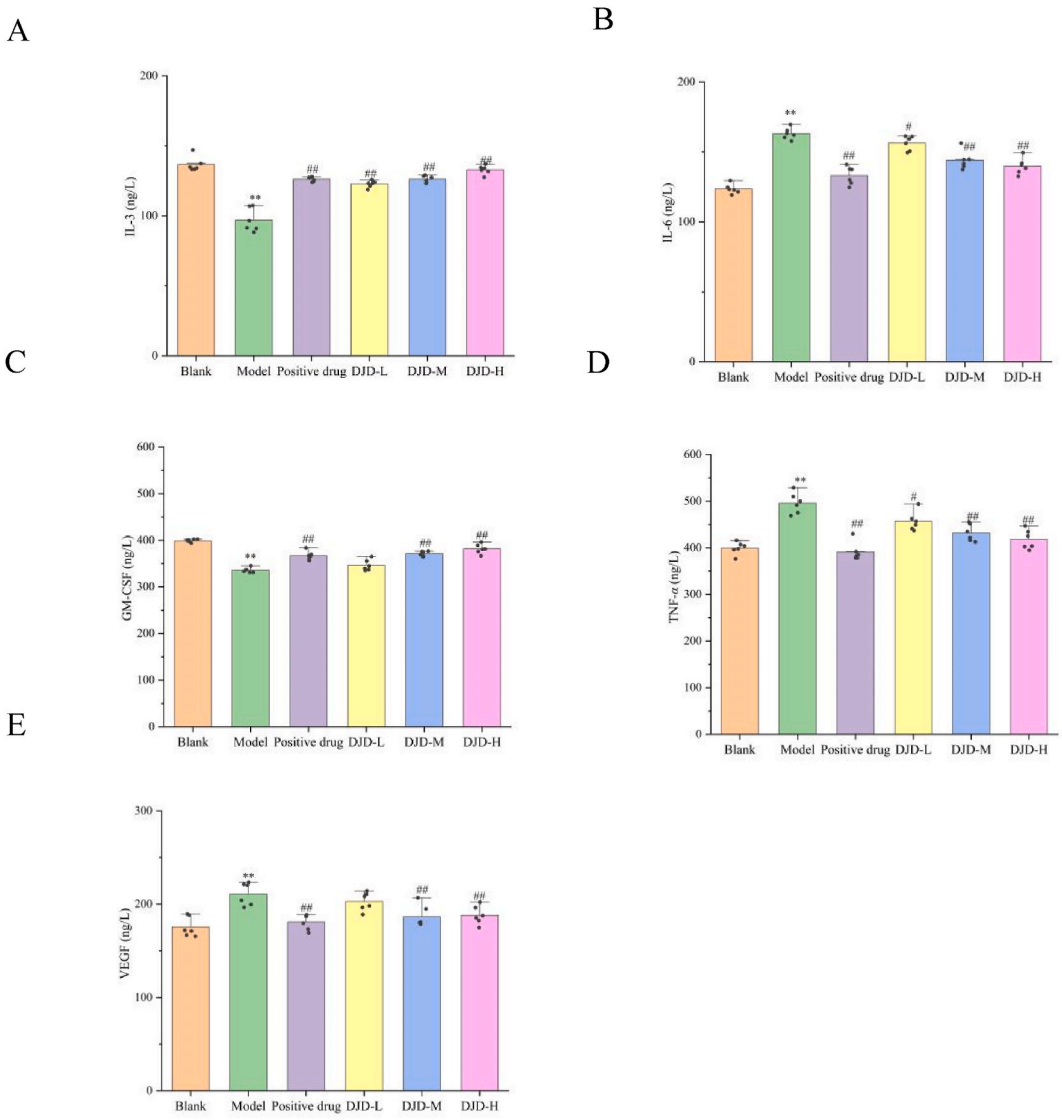

Fig. 7. Effect of DJD on the expression of IL-3, IL-6, GM-SCF, TNF-α, and VEGF.

the model group, a total of 66 metabolites were identified, with 34 being up-regulated and 32 down-regulated, as depicted in Fig. 9A and B. In the comparison between the DJD group and the model group, a total of 75 metabolites were identified, with 41 up-regulated and 34 down-regulated, as shown in Fig. 9C and D. Metabolites that exhibited significant changes and could be significantly regulated by DJD in the model group, compared with the blank group, were considered differential metabolites. After thorough screening and matching, 10 different metabolites related to MAC metabolism were identified, as presented in Table 1.

3.7.3. Enrichment analysis of metabolic pathways

Metabolic pathways associated with differential metabolites were investigated using the MetaboAnalyst 5.0 database. The results, shown in Fig. 10, indicate that differential metabolites are primarily concentrated in pathways related to phenylalanine, tyrosine, and tryptophan biosynthesis, phenylalanine metabolism, and arachidonic acid metabolism. These findings suggest that DJD may improve MAC by regulating these metabolic pathways.

4. Discussion

TCM is extensively utilized in treating MAC owing to its low toxicity and favorable therapeutic effects. However, the intricate nature of TCM often obscures its therapeutic efficacy and mechanisms. In recent years, network pharmacology has gained prominence in the research of multi-component drugs, particularly in the analysis of compound preparations, by creating a unique "compound-target-disease" network [24]. Employing network pharmacology and molecular docking technology, this study screened the main

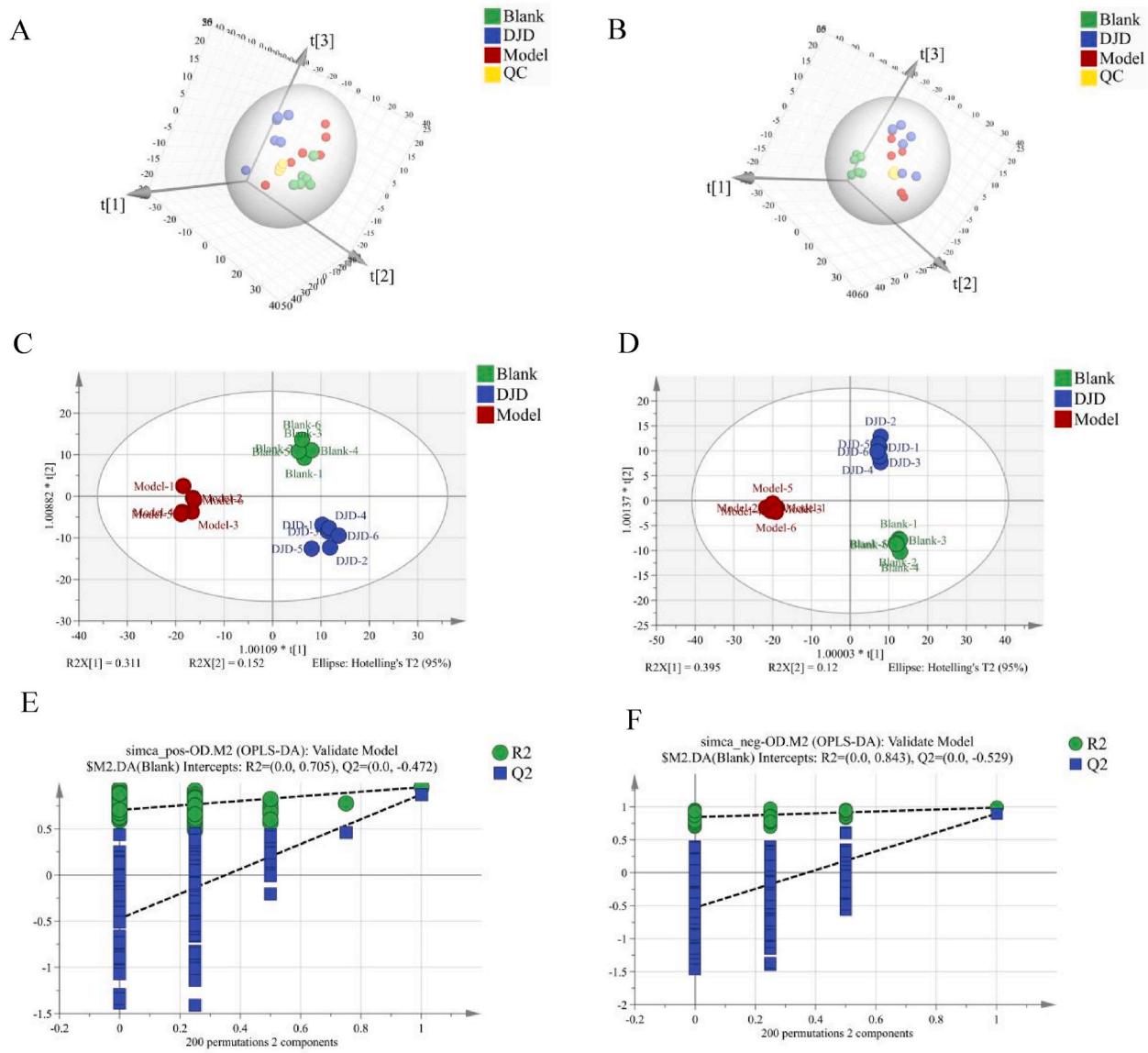

Fig. 8. Metabolomics profiling analysis of serum. (A) PCA score plots in positive ion mode; (B) PCA score plots in positive ion mode; (C) OPLS-DA score plots in positive ion mode; (D) OPLS-DA score plots in negative ion mode; (E) OPLS-DA validation plot in positive ion mode; (F) OPLS-DA validation plot in negative ion mode.

active compounds, action targets, and MAC-related targets of DJD using relevant software and data platforms. It also analyzed the potential action pathway of DJD in treating MAC. Common targets of DJD and MAC were identified using databases, revealing 201 drug targets for DJD, 3113 disease targets for MAC, and 95 intersecting targets of drugs and diseases. PPI analysis of DJD MAC-related targets via the STRING online database indicated that key proteins such as AKT1, STAT3, CASP3, and JUN were significantly associated with MAC. Molecular docking technology, which computationally simulates the interaction between drug molecules and targets, showed that the binding energy of each active component with different core proteins was less than −4 kcal/mol, indicating suitable docking effects.

The lack of selectivity in most cancer chemotherapy drugs and their primary side effect of inhibiting bone marrow hematopoietic stem cells results in MAC [25]. In this study, cyclophosphamide, commonly used in clinical settings, was employed to construct a MAC animal model. Cyclophosphamide can damage the bone marrow hematopoietic system, reduce peripheral blood cell counts, and affect the proliferation, differentiation, and metastasis of bone marrow hematopoietic stem cells. The successful establishment of the MAC animal model was evaluated by observing the number of peripheral blood cells. Changes in blood cell numbers reflect the impact of drugs on the hematopoietic function of MAC model animals. Experimental results indicated that the weight of rats in the model group decreased significantly, and the levels of WBCs, RBCs, HGB, and PLTs were significantly reduced, confirming the successful

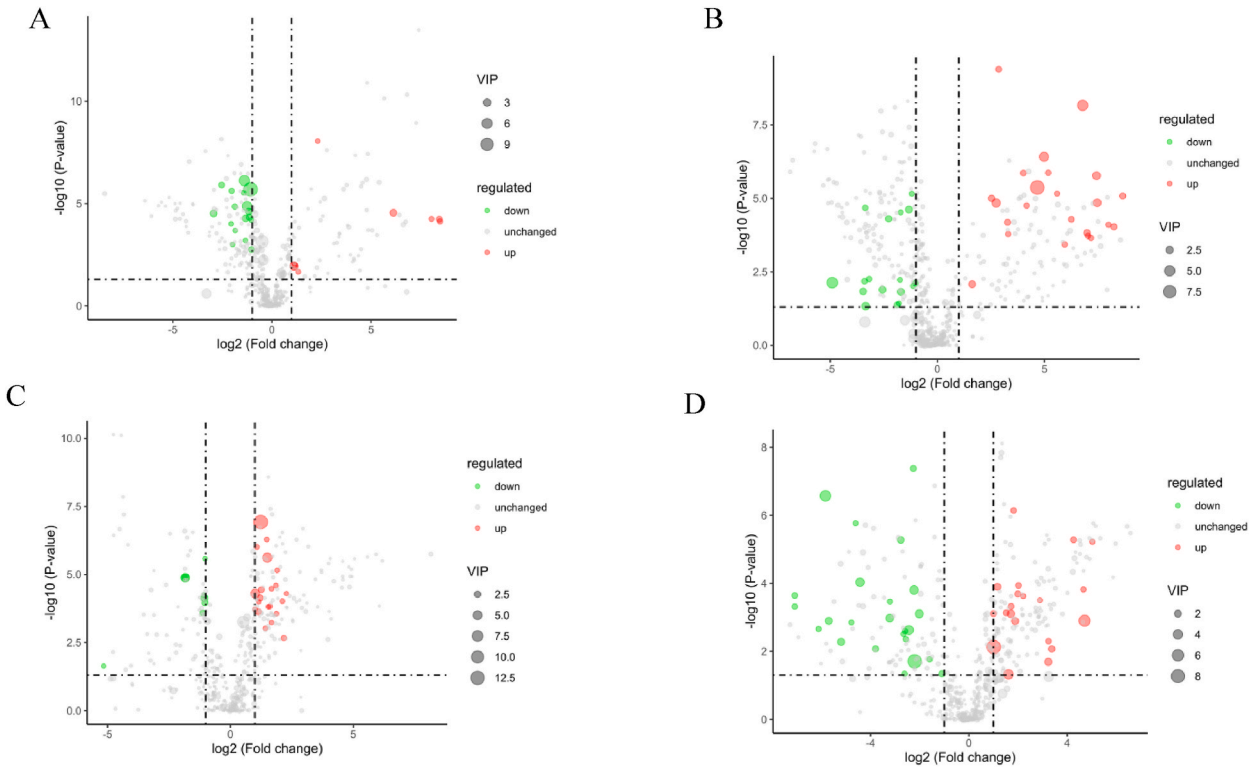

Fig. 9. Volcanic map of differential metabolites. (A) Blank group vs Model group in positive ion mode of differential metabolites; (B) Blank group vs Model group in negative ion mode of differential metabolites; (C) DJD group vs Model group in positive ion mode of differential metabolites; (D) DJD group vs Model group in negative ion mode of differential metabolites. The scatter size shows VIP value. The green dots represent differently expressed metabolites that are down-regulated, the red dots represent differentially expressed metabolites that are up-regulated, and the black dots represent discovered but unimportant metabolites.

Table 1
Identification results of potential biomarkers of serum samples in MAC rats.

No	Metabolite	Formula	RT/min	Experimental *m/z*	ESI mode	Trend	
						Blank VS Model	DJD VS Model
1	Choline	$C_5H_{13}NO$	0.78	103.099 99	+	↓##	↑**
2	Cytosine	$C_4H_5N_3O$	0.85	111.043 45	+	↓##	↑**
3	L-Phenylalanine	$C_9H_{11}NO_2$	2.05	165.078 86	+	↓#	↑**
4	Indoxyl sulfate	$C_8H_7NO_4S$	8.47	213.009 06	-	↓##	↑**
5	p-Cresol sulfate	$C_7H_8O_4S$	9.50	188.013 65	-	↓##	↑**
6	Cholic acid glucuronide	$C_{30}H_{48}O_{11}$	9.55	584.320 18	-	↓##	↑**
7	7-Ketodeoxycholic acid	$C_{24}H_{38}O_5$	10.28	406.272 07	-	↓##	↑**
8	Cholic acid	$C_{24}H_{40}O_5$	10.84	408.287 65	-	↓##	↑*
9	1-Stearoyl-*sn*-glycero-3-phosphocholine	$C_{26}H_{54}NO_7P$	14.20	523.363 03	+	↓##	↑**
10	Arachidonic acid	$C_{20}H_{32}O_2$	17.02	304.239 68	+	↓##	↑**

RT: Retention time; ESI: Electron spray ionization. $\#P < 0.05$, $\#\#P < 0.01$; $*P < 0.05$, $**P < 0.01$.

establishment of the MAC rat model.

Ejiao syrup is frequently used in clinical settings for patients with qi and blood deficiency, as it can improve the immune and hematopoietic functions of MAC model rats. Therefore, it was chosen as a positive control drug in this study [26]. In vivo experiments demonstrated that DJD possesses a therapeutic effect on MAC model rats. Post-DJD treatment, the survival rate of MAC model rats significantly improved, levels of WBCs, RBCs, HGB, and PLTs increased significantly, the level of RET decreased, and the size of the thymus and spleen gradually normalized. At the microscopic level of bone marrow, MAC model rats exhibited notable marrow cavitation with a proliferation of adipocytes, a significant decrease in hematopoietic-related cells, and evident pathological damage to the bone marrow. Intervention led to active bone marrow hyperplasia, dense distribution of nucleated cells, and a significant reduction in lipid droplets.

The proliferation and differentiation of bone marrow hematopoietic cells are outcomes of the coordinated action of various

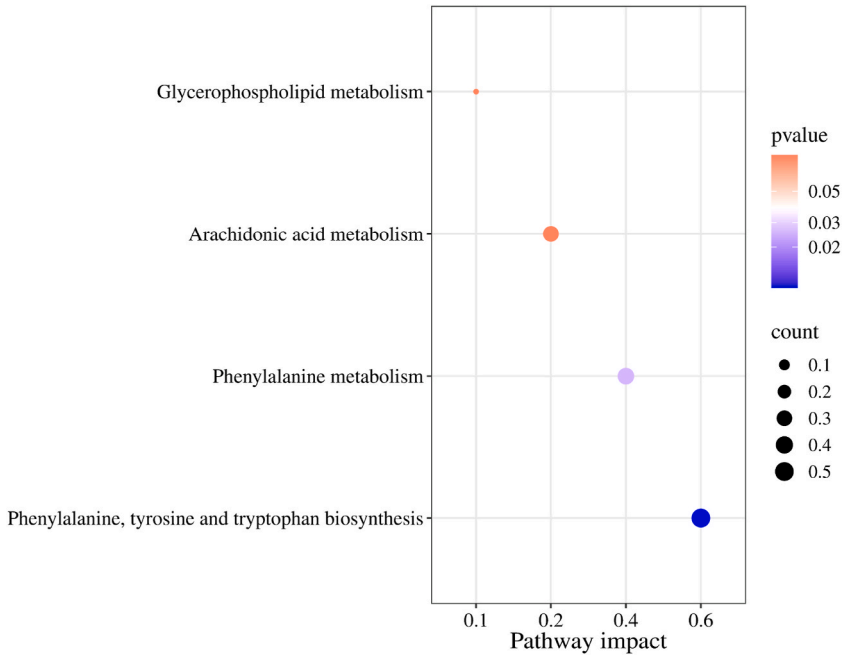

Fig. 10. Pathways of potential biomarkers related to pathogenesis of MAC.

hematopoietic growth factors within the hematopoietic microenvironment. GM-CSF, a pleiotropic hematopoietic growth factor in vivo, can stimulate the proliferation of early hematopoietic progenitor cells [27]. IL-3, a polyclonal hematopoietic growth factor, plays a crucial role in regulating the hematopoietic system as part of the immune system. It primarily influences the proliferation and differentiation of early and middle-stage hematopoietic progenitor cells. IL-3 and GM-CSF can synergistically promote hematopoiesis. IL-6, a cytokine secreted by bone marrow stromal cells, can induce the death of hematopoietic progenitor cells at very low concentrations. It also collaborates with IL-3 to stimulate DNA protein synthesis in megakaryocytes and encourage the development of megakaryocytes into mature platelets [28]. VEGF, known as a potent angiogenic factor, can promote angiogenesis, prevent endothelial cell apoptosis, regulate hematopoietic stem cell survival, and thereby influence hematopoietic function [29]. The results indicated that DJD significantly upregulated the expression of hematopoietic-related factors like GM-CSF and IL-3 and inhibited the secretion of inflammatory factors such as IL-6 and TNF-α. These findings suggest that DJD treats MAC through a multicomponent, multitarget, and multipathway approach.

The serum metabonomics results indicated that DJD could regulate endogenous substances like L-Phenylalanine, Arachidonic acid, Cholic acid, and Cholic acid glucuronide, which are involved in amino acid metabolism associated with bone marrow hematopoietic injury. L-asparagine primarily participates in the aspartic acid metabolism pathway. Research has shown that hematopoietic stem cells can enhance their function by increasing aspartic acid synthesis to synthesize asparagine and purine [30]. This study suggests that DJD may promote hematopoietic repair by regulating the synthesis and metabolism of various amino acids.

Additionally, the docking binding energy of the four active ingredients was found to be lowest with AKT1, highlighting the significance of AKT1 in treating MAC. The PI3K/AKT signaling pathway is crucial in the proliferation and differentiation of hematopoietic stem cells [31–33], and activation of this pathway has been shown to enhance hematopoietic function [34]. Furthermore, the PI3K/AKT signaling pathway is mediated by integrin (β1) subfamily adhesion molecules, whose abnormal expression is closely linked to damage in the hematopoietic microenvironment [35,36]. Thus, it is hypothesized that DJD decoction might improve hematopoietic microenvironment damage mediated by integrin VLA β1 by regulating the expression of AKT protein.

Given that DJD is widely used in clinical practice but lacks scientific research reports, this study represents the first application of network pharmacology combined with metabonomics technology to explore the material basis, pharmacological mechanism, and metabolic regulation of DJD in treating MAC. This approach is both a breakthrough and an innovative attempt. However, the limitations of this study are acknowledged, and further exploration into the mechanism of DJD in treating MAC is planned.

5. Conclusion

This study demonstrates that DJD exerts its therapeutic effects through multiple ingredients, targeting various pathways and biological targets. DJD potentially activates the PI3K/AKT signaling pathway, enhances the production of hematopoietic-related cytokines, regulates associated metabolic pathways, and effectively mitigates cyclophosphamide-induced myelosuppression after chemotherapy in rats.

Funding

This research did not receive any specific grant from funding agencies in the public, commercial, or not-for-profit sectors.

CRediT authorship contribution statement

Mingxin Guo: Writing – original draft, Validation. **Jiaqi Zeng:** Writing – original draft, Validation. **Wenjing Li:** Writing – review & editing, Resources, Conceptualization. **Zhiqiang Hu:** Supervision. **Ying Shen:** Formal analysis, Conceptualization.

Declaration of competing interest

The authors declare that they have no known competing financial interests or personal relationships that could have appeared to influence the work reported in this paper.

Acknowledgements

Thanks for the help of Tieliang Ma and Yaoxiang Sun.

Appendix A. Supplementary data

Supplementary data to this article can be found online at https://doi.org/10.1016/j.heliyon.2024.e24695.

References

[1] S. Yang, H. Che, L. Xiao, B.J. Zhao, S.S. Liu, Traditional Chinese medicine on treating myelosuppression after chemotherapy: a protocol for systematic review and meta-analysis, Medicine 100 (2021) e24307.
[2] S. Tsuboi, T. Hayama, K. Miura, A. Uchiike, D. Tsutsumi, T. Yamauchi, Y. Hatta, S. Ootsuka, Higher incidence of pegfilgrastim-induced bone pain in younger patients receiving myelosuppressive chemotherapy: a real-world experience, J. Pharm. Health Care Sci. 9 (2023) 2.
[3] X.Q. Huo, Y. Gu, Y.L. Zhang, The discovery of multi-target compounds with anti-inflammation activity from traditional Chinese medicine by TCM-target effects relationship spectrum, J. Ethnopharmacol. 293 (2022) 115289.
[4] L. Zhu, R. Chen, Analysis of clinical medication in the treatment of frozen shoulder by Jiawei Danggui Jixueteng decoction, Digital Chinese Medicine Branch Inaugural Meeting of International Digital Medicine Association and the First Digital Chinese Medicine Academic Exchange Conference (2016).
[5] X.D. Yu, S.G. Liu, X.L. Gao, H. Chen, Flavored angelica caulis spatholobi decoction exerts estrogen-like effects to protect bone loss in ovariectomized rats, Chin. J. Osteoporos. 28 (2022) 1024–1028, 1050.
[6] M. Dawra, J. Bouajila, M. El Beyrouthy, A.A. Rizk, P. Taillandier, N. Nehme, Y.E. Rayess, Chemical characterization and antioxidant, antibacterial, antiacetylcholinesterase and antiproliferation properties of salvia fruticosa miller extracts, Molecules 28 (2023) 2429.
[7] Y. Gao, Y. Zhang, W. Liu, N. Zhang, Q. Gao, J. Shangguan, N. Li, Y. Zhao, Y. Jia, Danggui Buxue decoction alleviates cyclophosphamide-induced myelosuppression by regulating β-hydroxybutyric acid metabolism and suppressing oxidative stress, Pharm. Biol. 61 (2023) 710–721.
[8] C. Cui, M. Xia, J. Chen, B. Shi, C. Peng, H. Cai, L. Jin, R. Hou, 1H NMR-based metabolomics combined with chemometrics to detect edible oil adulteration in huajiao (Zanthoxylum bungeanum Maxim.), Food Chem. 423 (2023) 136305.
[9] Y.L. Sun, P.P. Zhao, C.B. Zhu, M.C. Jiang, X.M. Li, J.L. Tao, C.C. Hu, B. Yuan, Integrating metabolomics and network pharmacology to assess the effects of quercetin on lung inflammatory injury induced by human respiratory syncytial virus, Sci. Rep. 13 (2023) 8051.
[10] K. Wang, J. Ma, Y. Li, Q. Han, Z. Yin, M. Zhou, M. Luo, J. Chen, S. Xia, Effects of essential oil extracted from Artemisia argyi leaf on lipid metabolism and gut microbiota in high-fat diet-fed mice, Front. Nutr. 9 (2022) 1024722.
[11] W. Feng, C. Duan, F. Pan, C. Yan, H. Dong, X. Wang, J. Zhang, Integration of metabolomics and network pharmacology to reveal the protective mechanism underlying Wogonoside in acute myocardial ischemia rats, J. Ethnopharmacol. 317 (2023) 116871.
[12] J. Ru, P. Li, J. Wang, W. Zhou, B. Li, C. Huang, P. Li, Z. Guo, W. Tao, Y. Yang, X. Xu, Y. Li, Y. Wang, L. Yang, TCMSP: a database of systems pharmacology for drug discovery from herbal medicines, J. Cheminf. 6 (2014) 13.
[13] A. Daina, O. Michielin, V. Zoete, SwissTargetPrediction: updated data and new features for efficient prediction of protein targets of small molecules, Nucleic Acids Res. 2019 47 (2019) W357–W364.
[14] D. Xu, L. Cai, S. Guo, L. Xie, M. Yin, Z. Chen, H. Zhou, Y. Su, Z. Zeng, X. Zhang, Virtual screening and experimental validation identify novel modulators of nuclear receptor RXRα from Drugbank database, Bioorg. Med. Chem. 27 (2017) 1055–1061, 459.
[15] A.P. Davis, C.J. Grondin, R.J. Johnson, D. Sciaky, B.L. King, R. McMorran, J. Wiegers, T.C. Wiegers, C.J. Mattingly, The comparative toxicogenomics database: update 2017, Nucleic Acids Res. 45 (2017) D972–d978.
[16] M. Rebhan, V. Chalifa-Caspi, J. Prilusky, D. Lancet, GeneCards: integrating information about genes, proteins and diseases, Trends Genet. TIG. 13 (1997) 163.
[17] W. Zhang, A. Bojorquez-Gomez, D.O. Velez, G. Xu, K.S. Sanchez, J.P. Shen, K. Chen, K. Licon, C. Melton, K.M. Olson, M.K. Yu, J.K. Huang, H. Carter, E.K. Farley, M. Snyder, S.I. Fraley, J.F. Kreisberg, T. Ideker, A global transcriptional network connecting noncoding mutations to changes in tumor gene expression, Nat. Genet. 50 (2018) 613–620.
[18] Y. Wang, S. Zhang, F. Li, Y. Zhou, Y. Zhang, Z. Wang, R. Zhang, J. Zhu, Y. Ren, Y. Tan, C. Qin, Y. Li, X. Li, Y. Chen, F. Zhu, Therapeutic target database 2020: enriched resource for facilitating research and early development of targeted therapeutics, Nucleic Acids Res. 48 (D1) (2020) D1031–D1041.
[19] C.Y. Yan, X. Li, G.L. Zhang, J. Bi, H. Hao, H. Hou, Quorum Sensing (QS)-regulated target predictions of Hafnia alvei H4 based on the joint application of genome and STRING database, Food Res. Int. 157 (2022) 111356.
[20] D. Seeliger, B.L. de Groot, Ligand docking and binding site analysis with PyMOL and Autodock/Vina, J. Comput. Aided Mol. Des. 24 (2010) 417–422.
[21] B. Hu, P. Das, X. Lv, M. Shi, J. Aa, K. Wang, L. Duan, J.A. Gilbert, Y. Nie, X.L. Wu, Effects of 'healthy' fecal microbiota transplantation against the deterioration of depression in fawn-hooded rats, mSystems 7 (3) (2022) e21822.
[22] M. Li, Y. Qiu, M. Guo, R. Qu, F. Tian, G. Wang, Y. Wang, J. Ma, S. Liu, H. Takiff, Y.W. Tang, Q. Gao, Evaluation of the Cepheid 3-gene host response blood test for tuberculosis diagnosis and treatment response monitoring in a primary-level clinic in rural China, J. Clin. Microbiol. 30 (2023) e0091123.

[23] M.F. Du, X. Zhang, G.L. Hu, J.J. Mu, C. Chu, Y.Y. Liao, C. Chen, D. Wang, Q. Ma, Y. Yan, H. Jia, K.K. Wang, Y. Sun, Z.J. Niu, Z.Y. Man, L. Wang, X.Y. Zhang, W. J. Luo, W.H. Gao, H. Li, G.J. Wu, K. Gao, J. Zhang, Y. Wang, Associations of lipid accumulation product, visceral adiposity index, and triglyceride-glucose index with subclinical organ damage in healthy Chinese adults, Front. Endocrinol. 14 (2023) 1164592.
[24] H. Hu, H. Wang, X. Yan, Z. Li, W. Zhan, H. Zhu, T. Zhang, Network pharmacology analysis reveals potential targets and mechanisms of proton pump inhibitors in breast cancer with diabete, Sci. Rep. 2023 13 (2023) 7623.
[25] H.L. Zhan, Y.J. Bai, Y. Lv, X. Zhang, L. Zhang, S. Deng, Pharmacological mechanism of mylabris in the treatment of leukemia based on bioinformatics and systematic pharmacolog, Bioengineered 12 (2021) 3229–3239.
[26] W. Li, Y. Wang, J. Han, J. Zhang, B. Li, X. Qi, Y. Zhang, F. Hu, H. Liu, UPLC-Q-TOF-MS and UPLC-QQQ-MS were used for the qualitative and quantitative analysis of oligosaccharides in Fufang Ejiao Syrup, J. Pharm. Biomed. Anal. 224 (2023) 115193.
[27] G.N. Cox, J.I. Lee, M.S. Rosendahl, E.A. Chlipala, D.H. Doherty, Characterization of a long-acting site-specific PEGylated murine GM-CSF analog and analysis of its hematopoietic properties in normal and cyclophosphamide-treated neutropenic rats, Protein J. 39 (2020) 160–173.
[28] S. Khaseb, A. Atashi, S. Kaviani, M. Rezai Rad, M. Ajami, M. Ajami, Expression analysis of genes involved in the expansion of hematopoietic stem cells (SCF, Flt3-L, TPO, IL-3, and IL-6) in unrestricted somatic stem cells cultured on fibrin, Biochimie 212 (2023) 135–142.
[29] Y. Zhang, Y. Cao, Y. Li, L. Xiao, W. Xu, W. Xu, M. Huang, X. Zhang, Y. Chen, L. Nan, Gualou Guizhi decoction promotes therapeutic angiogenesis via the miR210/HIF/VEGF pathway in vivo and in vitro, Pharmaceut. Biol. 61 (1) (2023) 779–789.
[30] L. Qi, M.S. Martin-Sandoval, S. Merchant, W. Gu, M. Eckhardt, T.P. Mathews, Z. Zhao, M. Agathocleous, S.J. Morrison, Aspartate availability limits hematopoietic stem cell function during hematopoietic regeneration, Cell Stem Cell 28 (2021) 1982–1999.
[31] I. Khan, Z. Huang, Q. Wen, M.J. Stankiewicz, L. Gilles, B. Goldenson, R. Schultz, L. Diebold, S. Gurbuxani, C.M. Finke, T.L. Lasho, P. Koppikar, A. Pardanani, B. Stein, J.K. Altman, R.L. Levine, A. Tefferi, J.D. Crispino, AKT is a therapeutic target in myeloproliferative neoplasms, Leukemia 27 (9) (2013) 1882–1890.
[32] M.G. Kharas, R. Okabe, J.J. Ganis, M. Gozo, T. Khandan, M. Paktinat, D.G. Gilliland, K. Gritsman, Constitutively active AKT depletes hematopoietic stem cells and induces leukemia in mice, Blood, The Journal of the American Society of Hematology 115 (7) (2010) 1406–1415.
[33] Y. Zhang, T. Ye, Z. Hong, S. Gong, X. Zhou, H. Liu, J. Qian, H. Qu, Pharmacological and transcriptome profiling analyses of Fufang E'jiao Jiang during chemotherapy-induced myelosuppression in mice, J. Ethnopharmacol. 238 (2019) 111869.
[34] M. Zeng, Y. Zhang, X. Zhang, W. Zhang, Q. Yu, W. Zeng, D. Ma, J. Gan, Z. Yang, X. Jiang, Two birds with one stone: YQSSF regulates both proliferation and apoptosis of bone marrow cells to relieve chemotherapy-induced myelosuppression, J. Ethnopharmacol. 289 (2022) 115028.
[35] A. Rashidi, G.L. Uy, Targeting the microenvironment in acute myeloid leukemia, Curr. Hematol. Malig. R. 10 (2015) 126–131.
[36] Y. Shiozawa, K.J. Pienta, R.S. Taichman, Hematopoietic stem cell niche is a potential therapeutic target for bone metastatic tumors, Clin. Cancer Res. 17 (17) (2011) 5553–5558.